

Review

# Breaking of Odd Chirality in Magneto-electrodeposition

Iwao Mogi <sup>1,\*</sup> , Ryoichi Morimoto <sup>2</sup> , Ryoichi Aogaki <sup>3</sup> and Kohki Takahashi <sup>1</sup>

<sup>1</sup> Institute for Materials Research, Tohoku University, Katahira, Aoba-ku, Sendai 980-8577, Japan; kohki@imr.tohoku.ac.jp

<sup>2</sup> SAITEC, Kawaguchi, Saitama 333-0844, Japan; morimotoryoichi@mbn.nifty.com

<sup>3</sup> Department of Product Design, Polytechnic University, Sumida, Tokyo 130-0026, Japan; ryoochan@aol.com

\* Correspondence: iwao.mogi.d4@tohoku.ac.jp

**Abstract:** Electrodeposition under magnetic fields (magneto-electrodeposition; MED) can induce surface chirality on copper films. The chiral signs of MED films should depend on the magnetic field polarity; namely, the reversal of the magnetic field causes the opposite chiral sign. This represents odd chirality for the magnetic field polarity. However, odd chirality was broken in several MED conditions. This paper makes a survey of breaking of odd chirality in the MED conditions such as low magnetic fields, specific adsorption of chloride ions, micro-electrode, and cell rotation. These results indicate that the ordered fluctuation of magnetohydrodynamic micro-vortices induces the breaking of odd chirality and that the random fluctuation results in the disappearance of surface chirality.

**Keywords:** electrodeposition; magnetic field; surface chirality; micro-MHD vortex; symmetry breaking; fluctuation



**Citation:** Mogi, I.; Morimoto, R.; Aogaki, R.; Takahashi, K. Breaking of Odd Chirality in Magneto-electrodeposition. *Magnetochemistry* **2022**, *8*, 67. <https://doi.org/10.3390/magnetochemistry8070067>

Academic Editors: Evgeny Katz, Anne-Lise Daltin and Xuegeng Yang

Received: 9 May 2022

Accepted: 20 June 2022

Published: 23 June 2022

**Publisher's Note:** MDPI stays neutral with regard to jurisdictional claims in published maps and institutional affiliations.



**Copyright:** © 2022 by the authors. Licensee MDPI, Basel, Switzerland. This article is an open access article distributed under the terms and conditions of the Creative Commons Attribution (CC BY) license (<https://creativecommons.org/licenses/by/4.0/>).

## 1. Introduction

The imposition of magnetic fields on electrochemical cells causes magnetohydrodynamic (MHD) flows in electrolytic solutions [1–12]. One of the most remarkable effects of MHD flows is to induce spiral and helical structures of metals [13–23], metal silicates [24,25], and conducting polymers [26,27] in magneto-electrodeposition (MED). The chirality of these structures depended on the magnetic field polarity, namely, the reversal of imposed magnetic field brought about the opposite chirality of electrodeposits. This relation represents “odd chirality” for the magnetic field polarity [28].

The above chiral structures were on macroscopic scales of mm and cm. Chiral structures on molecular scales have been explored in the MED methods [29–32]. We found that the MED of metal films induces the surface chirality of silver [33,34] and copper films [35,36], which recognized the molecular chirality of glucose [33], amino acids [35], and tartaric acid [37].

The chiral surface formation in the MED processes takes place at the configuration where the imposed magnetic field is perpendicular to the working electrode surface. Figure 1 shows two types of MHD flows around the electrode [38–40]. With the elapse of time during electrodeposition, the non-equilibrium fluctuation causes bumps and pits on the film surfaces. Micro-MHD vortices are excited at such local sites, and the adjoining vortices have opposite directions to each other, forming symmetrical self-organized states. The MED film surfaces have circular or network structures reflecting the micro-MHD vortices [35,38,41]. On the other hand, another macroscopic flow is excited around the electrode edge, where the ionic currents are not parallel to the magnetic field. This is termed a vertical MHD flow, which affects the micro-MHD vortices. The vertical MHD flow makes the cyclonic vortices stable, whereas it makes anticyclonic ones unstable [42,43]. There exist a number of screw dislocations on the film surfaces of electrodeposits of copper [44], which could be a chiral site. The micro-MHD vortices affect the formation of screw dislocations. The vertical MHD flow breaks the symmetry of the self-organized state of micro-MHD vortices, leading to chiral surface formation [39]. The direction of vertical MHD flow depends

on the magnetic field polarity; thus, the MED film surfaces should have odd chirality for the magnetic field polarity.

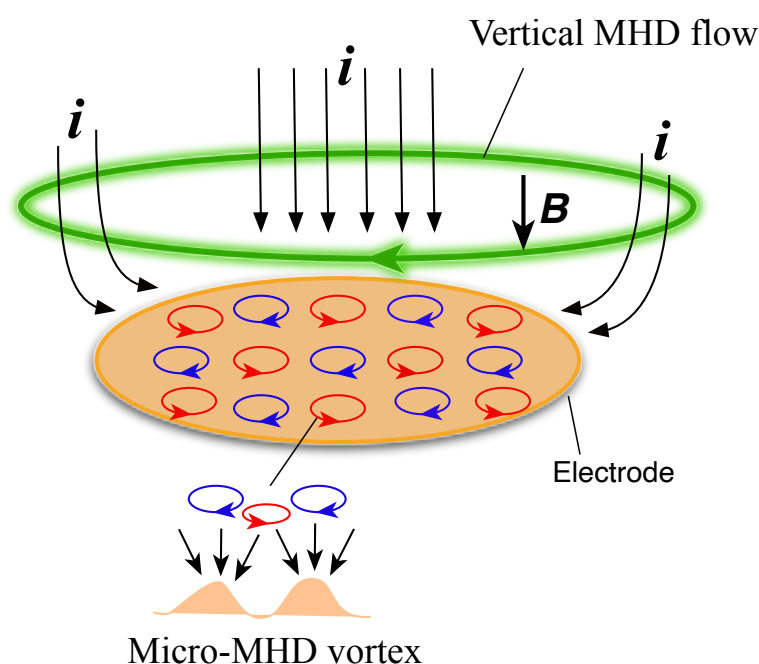


**Figure 1.** Self-organized state of micro-MHD vortices under the vertical MHD flow in a MED process with vertical magnetic fields  $B$ .

In the MED studies of copper films, the odd chirality has been observed at a high magnetic field of 5 T with a usual size (3 mm) electrode [35,45]. The rigid self-organized states of micro-MHD vortices under the vertical MHD flows can be formed in such a condition. Breaking of odd chirality has been found in the MED with an additive of potassium chloride even at 5 T [45]. The specific adsorption of chloride ions on the copper film surfaces disturbs the rigid formation of the micro-MHD vortices. This result suggests that the fluctuation of micro-MHD vortices could play a significant role in the breaking of odd chirality. This paper reviews the odd chiral behaviors of MED films in various conditions disturbing the micro-MHD states; low magnetic fields [46], chloride additives [45], micro-electrodes [47,48], and cell rotation [49,50]. The overview of MED conditions causing the breaking of odd chirality would lead to intrinsic factors for the chiral symmetry breaking.

Chiral surfaces could be used as a chiral catalyst, which plays an indispensable role in the pharmaceutical industry. In the early stage of earth, chiral surfaces of minerals could serve as catalytic reaction fields for the formation of amino acids in the molecular evolution toward the origin of life [51]. Therefore, it is of great significance to study the chiral surface formation and the breaking of chiral symmetry. The MED processes provide attractive experimental cases for such studies.

## 2. Materials and Methods

### 2.1. Experimental Methods of MED

The basic method of MED for chiral surface formation is depicted in Figure 2. The electrochemical cell was placed at the bore center of a solenoidal cryocooled superconducting magnet (Sumitomo Heavy Industries Ltd., Tokyo, Japan), which can generate magnetic fields of up to 5 T in a 220 mm room-temperature bore. The magnetic fields ( $B$ ) were imposed perpendicularly to the working electrode surface, and they are parallel ( $+B$ ) or antiparallel ( $-B$ ) to the ionic currents. The temperature within the magnet bore was thermoregulated at 25 °C by water circulation.

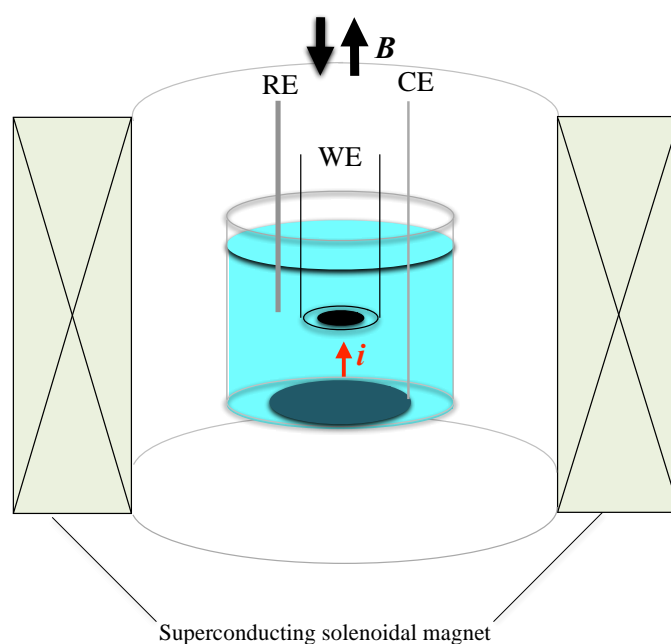


**Figure 2.** Configuration of an electrodeposition cell in a superconducting magnet in the MED experiments [35]. WE: a working electrode, CE: a counter electrode, and RE: a reference electrode.

The surface chirality was studied in the MED films of copper. The electrodeposition cell consisted of three electrodes: a working electrode was a polycrystalline platinum disc with a diameter of 3 mm (ALS Co., Ltd., Tokyo, Japan). A counter electrode was a copper plate, and a reference one was a  $\text{Ag} | \text{AgCl} | 3 \text{ M (M = mol dm}^{-3}\text{) NaCl}$  electrode. When the effects of micro-electrodes were examined, platinum micro-discs with diameters of 100 and 25  $\mu\text{m}$  (ALS Co., Ltd., Tokyo, Japan) were used as a working electrode. The electrolytic solution was a 50 mM  $\text{CuSO}_4 + 0.5 \text{ M H}_2\text{SO}_4$  aqueous solution. When the effects of chloride additives were examined, KCl was added to the electrolytic solution with concentrations of 0.10–0.26 mM.

The MED of copper films was conducted on a galvanostatic mode with constant currents of  $5\text{--}40 \text{ mA cm}^{-2}$ . The total passing charge was always  $0.4 \text{ C cm}^{-2}$ , then the film thickness was approximately 150 nm. The MED films prepared in +5T, for instance, were termed +5T films.

### 2.2. Experimental Methods of Rotational MED (RMED)

The cell rotation in the MED process is one of the most efficient methods for chiral surface formation. The electrodeposition cell was rotated in the magnet bore by a geared motor system with a bevel gear and a non-magnetic stainless-steel shaft. The detailed schematic is reported in the previous paper [50]. The rotational manners were 0.5–6 Hz frequencies and the clockwise (CW) or anticlockwise (ACW) directions. To suppress the influence of vertical MHD flows, the copper working electrode was embedded in a tube wall. The RMED was conducted on a potentiostatic mode at a constant potential of  $-0.45 \text{ V}$  (vs. Cu) with various rotational frequencies. The RMED films prepared in  $\pm 5\text{T}$  with the CW and ACW 6 Hz rotations, for instance, are termed {5T,6 Hz} films.

### 2.3. Estimation of Surface Chirality

The surface chirality of MED films was estimated by the voltammetric measurements of the enantiomers of alanine on the MED film electrodes [52–55]. The voltammograms of 20 mM L- and D-alanines were measured in a 0.1 M NaOH aqueous solution with a potential sweep rate of  $10 \text{ mV s}^{-1}$  just after the MED film preparation.

The enantiomeric excess ( $ee$ ) ratio, which serves as a chirality index, was defined as Equation (1) in terms of voltammetric parameters [45].

$$ee = (i_p^L - i_p^D)/(i_p^L + i_p^D), \quad (1)$$

where  $i_p^L$  and  $i_p^D$  represent the peak currents of L- and D-alanines, respectively. The positive and negative signs of  $ee$  ratios stand for L- and D-activity of the MED films, respectively.

### 3. Results and Discussion

#### 3.1. Odd Chirality and Effects of Low Magnetic Fields

The formation of the self-organized state of micro-MHD vortices in Figure 1 depends on the magnetic field. The rigid self-organized state can be formed in 5 T on a usual size (3 mm diameter) electrode, exhibiting the odd chirality of 5T films [45]. Figure 3a shows the voltammograms of L- and D-alanines on the +5T film electrodes prepared at the deposition current of  $20 \text{ mA cm}^{-2}$ . Both voltammograms show current peaks around 0.7 V, where alanine molecules are oxidized on the copper film electrodes [56]. The +5T film surfaces recognize the molecular chirality of alanine and exhibit the difference in peak currents. The greater peak current of L-alanine represents the L-activity of the film surface, meaning that the number of L-active sites is greater than that of D-active sites. On the other hand, the −5T film exhibits the D-activity, as shown in Figure 3b.

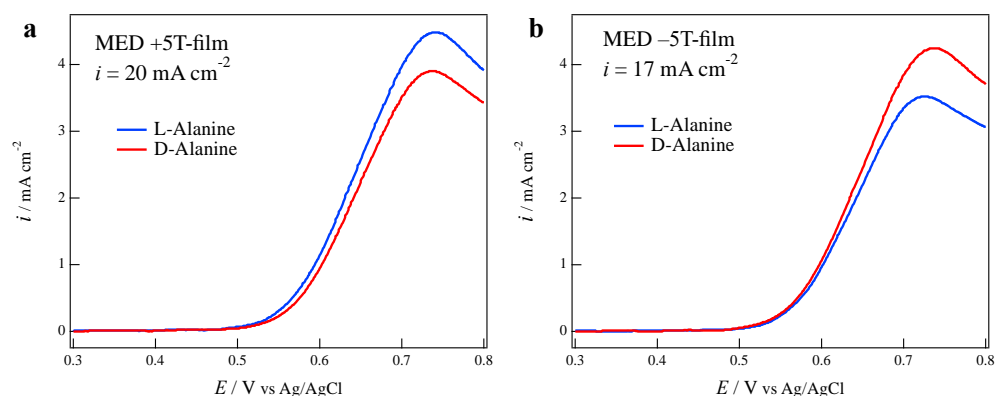


**Figure 3.** Voltammograms of alanine enantiomers in a 0.1 M NaOH aqueous solution on the MED film electrodes: (a); +5T films and (b); −5T films. Adopted from [46].

The  $ee$  ratios of MED films were plotted as a function of deposition current ( $ee$  ratio profile). Figure 4a,b show the  $ee$  ratio profiles of the +5T and −5T films, respectively. The +5T films show the D-activity at the low current region and L-activity at the high current one. On the contrary, the −5T films show the L-activity at the low current region and D-activity at the high current one. These facts can be described as Equation (2) and represent clear odd chirality for the magnetic field polarity.

$$ee(\mathbf{B}) \approx -ee(-\mathbf{B}). \quad (2)$$

As the magnetic field decreases, the weaker Lorentz force causes the fluctuation of micro-MHD vortices and disturbs the rigid formation of the self-organized micro-MHD state. Figure 4c,d show the  $ee$  ratio profiles of the +2T and −2T films, respectively [46]. Both films exhibit D-activity around  $9 \text{ mA cm}^{-2}$ , and this result represents the breaking of odd chirality. Similar broken odd chirality was observed in the 2.5T films [46]. When the magnetic field was lower, the micro-MHD vortices could not be excited enough to form the self-organized state; thus, the surface chirality disappeared in the 1T films.

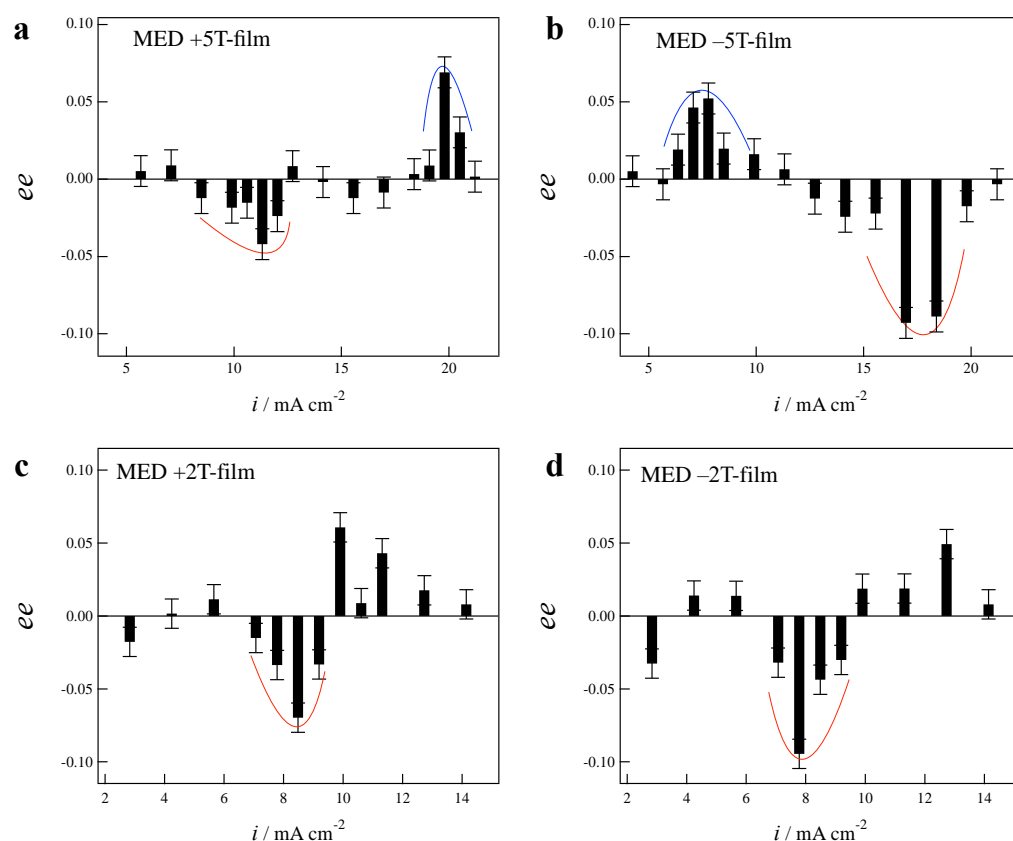


**Figure 4.** The  $ee$  ratio profiles of MED films: (a); +5T films, (b); -5T films, (c); +2T films, and (d); -2T films. Blue and red curves are a guide for the eyes. Adopted from [46].

### 3.2. Effects of Chloride Additives

Chloride ions are a typical inorganic additive in the electroplating of copper films for the formation of flat and smooth surfaces through the specific adsorption on the film surfaces [57–60]. Such adsorption can be expected to disturb the self-organized micro-MHD state, as shown in Figure 5, and affect the surface chirality of MED films.

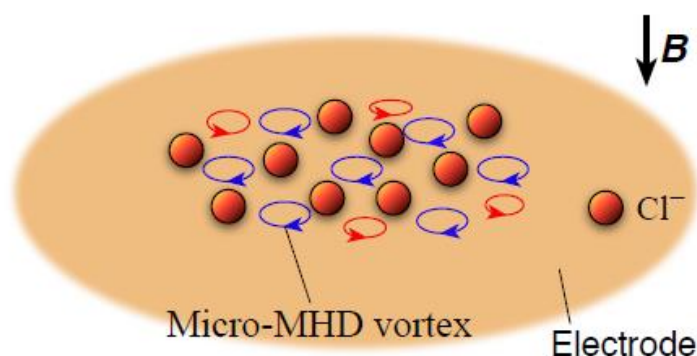


**Figure 5.** Schematic of the specific adsorption of chloride ions and the fluctuation of micro-MHD vortices on copper film surfaces.

The previous paper [45] reported the influence of chloride additives on the chiral behaviors of 5T films at the chloride concentration of 0.1–0.26 mM. The 5T films showed odd chirality at 0.10 mM, breaking of odd chirality at 0.13 and 0.20 mM, and achirality at 0.26 mM.

Here we show the combined effects of chloride additives and low magnetic fields on the chiral behaviors of MED films. Figure 6 shows the  $ee$  ratio profiles of 5T, 3T, and

2T films at the chloride concentration of 0.10 mM. The +5T films show D-activity in the whole current region (Figure 6a), and the −5T films show the L-activity (Figure 6b). This represents clear odd chirality. With decreasing magnetic field, the +3T films show D-activity in the low current region and L-activity in the high region (Figure 6c), whereas the −3T films show almost achirality (Figure 6d). Thus, the 3T films represent the breaking of odd chirality. At the lower magnetic field, both +2T and −2T films show achirality (Figure 6e,f).

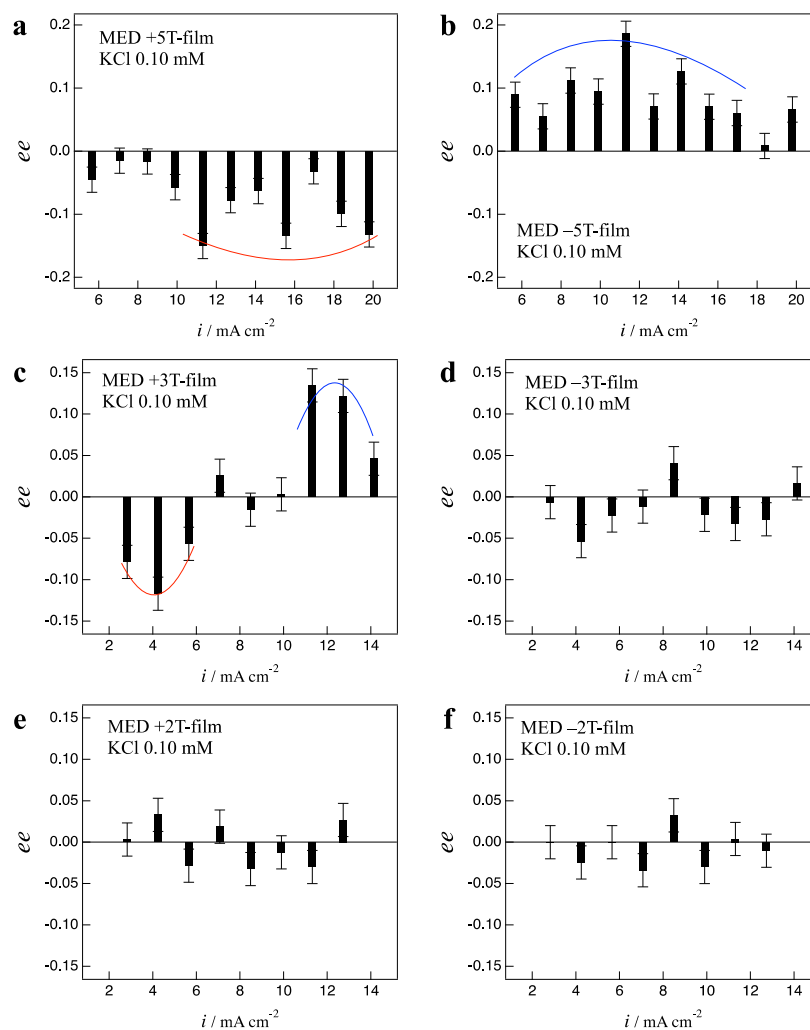
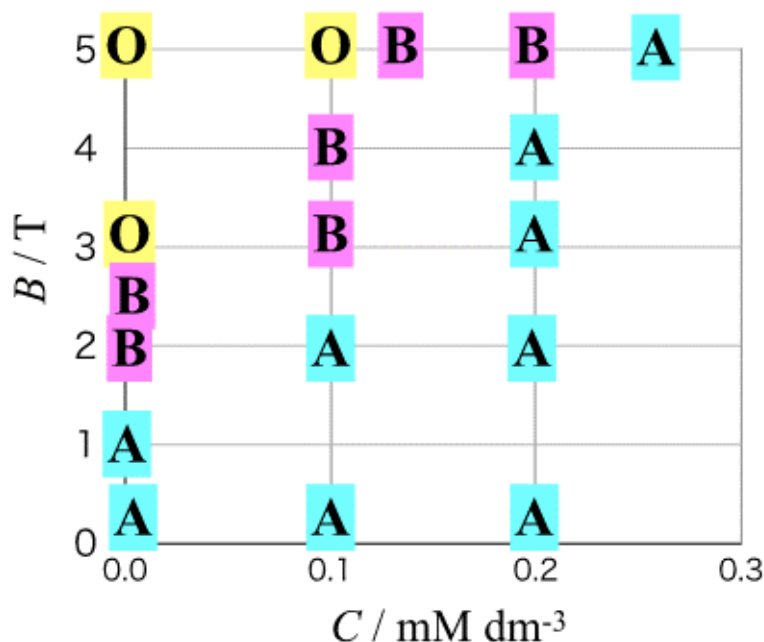


**Figure 6.** The  $ee$  ratio profiles of MED films prepared with 0.10 mM KCl: (a); +5T films, (b); −5T films, (c); +3T films, (d); −3T films, (e); +2T films, and (f); −2T films. Blue and red curves are a guide for eyes.

Similar MED experiments were conducted at the chloride concentration of 0.2 mM. The 5T films showed breaking of odd chirality, and the 4T, 3T, and 2T films showed achirality. The chloride adsorption induces the fluctuation of micro-MHD vortices and disturbs odd chirality even in the 5T films. The superimposed effects of low magnetic fields and chloride adsorption led to the random fluctuation of micro-MHD vortices, resulting in achirality in the 4T, 3T, and 2T films.

The chiral symmetry is mapped on the axes of the magnetic field and chloride concentration  $C$ , as shown in Figure 7, where [O], [B], and [A] represent odd chirality, breaking of odd chirality, and achirality, respectively. The appearance of odd chirality is confined in a zone at high magnetic fields and low chloride concentrations, where the rigid self-organized state of micro-MHD vortices could be formed. The breaking of odd chirality takes place in the outer zone of odd chirality. This zone is also confined in specific conditions of slightly lower magnetic fields and slightly higher concentrations, where there exists the fluctuation

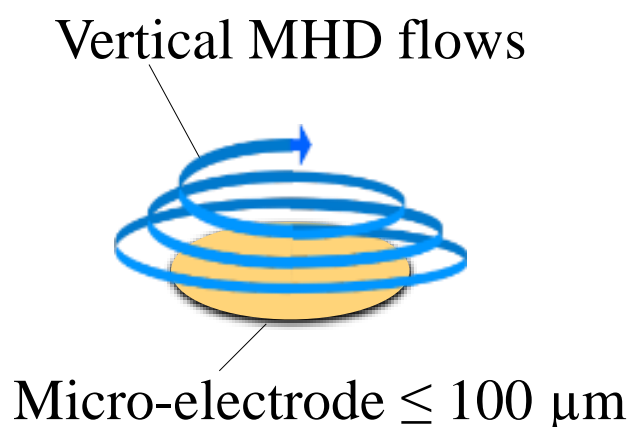
of micro-MHD vortices. Such fluctuation is not random but “ordered” so that the chiral surfaces can be formed. There is a wide zone of achirality, where both lower magnetic fields and higher chloride concentrations cause the random fluctuation of micro-MHD vortices.



**Figure 7.** Mapping of chiral symmetry on the axes of magnetic field vs. the concentration of chloride ions C. O: odd chirality; B: breaking of odd chirality; A: achirality.

### 3.3. Effects of Micro-Electrode

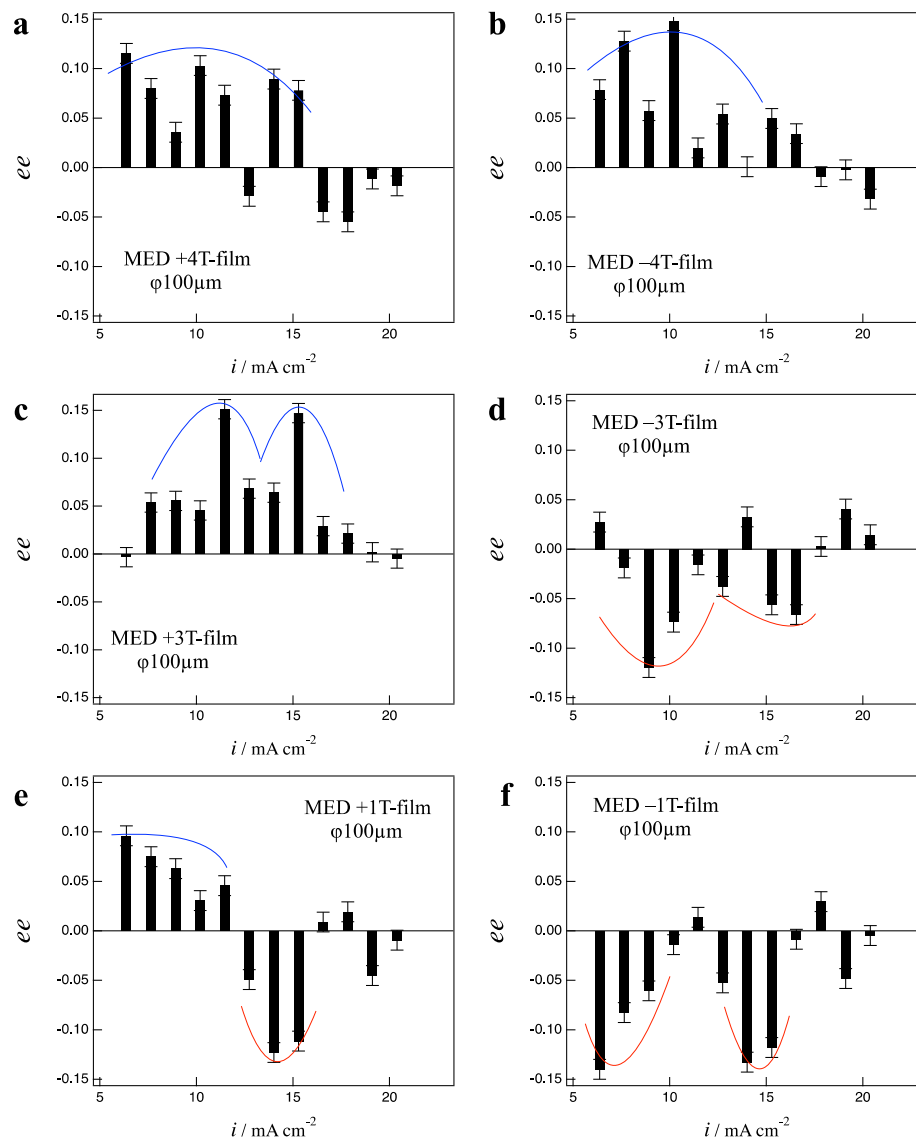
As the electrode size decreases to  $\mu\text{m}$  scales, the vertical MHD flows cover the whole area of the working electrode (Figure 8) and have considerable influence on the micro-MHD vortices. The chiral behaviors of MED films were examined on the electrodes with diameters of 100 and 25  $\mu\text{m}$  [47,48].



**Figure 8.** Schematic of the vertical MHD flows on a micro-electrode.

Figure 9 shows the *ee* ratio profiles of 4T, 3T, and 1T films on a 100  $\mu\text{m}$  electrode. Both +4T and -4T films show L-activity in the current region of 5–15  $\text{mA cm}^{-2}$  (Figure 9a,b). This broken odd chirality is due to the strong vertical MHD flows on the micro-electrode at 4T. This effect could be reduced in the lower magnetic fields. In Figure 9c,d, the +3T films show L-activity in the current region of 8–17  $\text{mA cm}^{-2}$ , and the -3T films show D-activity in the same region, representing clear odd chirality. When the magnetic field is lower, in the current region of 5–10  $\text{mA cm}^{-2}$  in Figure 9e,f, the +1T films show L-activity, and the

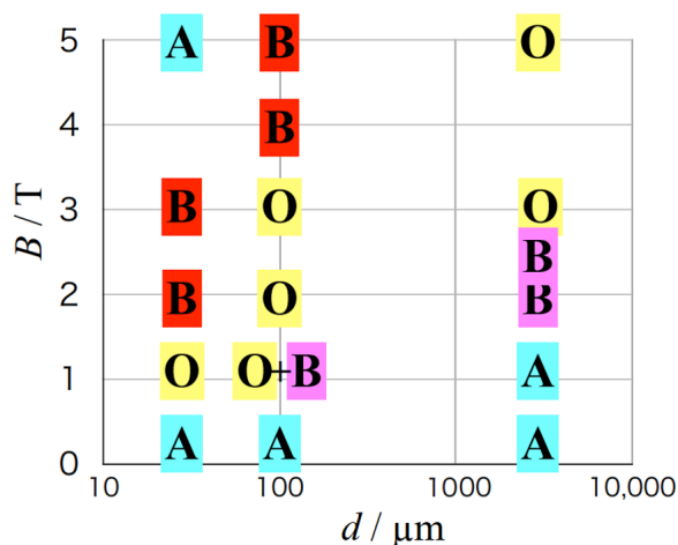
−1T film shows D-activity, representing odd chirality. On the other hand, both +1T and −1T films show D-activity around  $15 \text{ mA cm}^{-2}$ , representing broken odd chirality. Odd chirality and its breaking coexist in the 1T films. This broken odd chirality is due to the effects of low magnetic fields.



**Figure 9.** The  $ee$  ratio profiles of MED films prepared on a  $100 \mu\text{m}$  electrode: (a); +4T films, (b); −4T films, (c); +3T films, (d); −3T films, (e); +1T films, and (f); −1T films. Blue and red curves are a guide for the eyes. Adopted from [48].

Similar MED experiments were conducted on a  $25 \mu\text{m}$  electrode. The 5T films showed achirality, the 2T and 3T films showed broken odd chirality, and the 1T films showed odd chirality. This indicates that the drastic effects of vertical MHD flows on the  $25 \mu\text{m}$  electrode cause the random fluctuation of micro-MHD vortices in the 5T films.

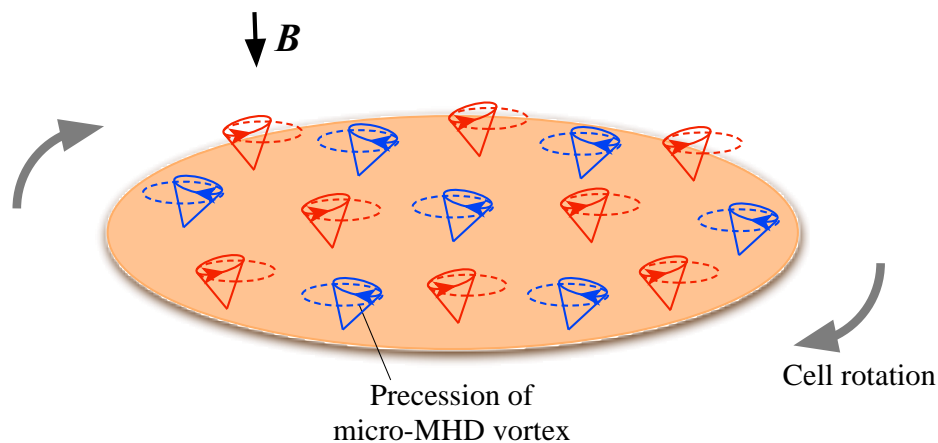
The chiral symmetry was mapped on the axes of magnetic field and electrode diameter  $d$  (logarithmic scales) as shown in Figure 10, which includes the results on a 3 mm electrode in Figure 7 (at  $C = 0 \text{ mM}$ ). Odd chirality appears on a confined zone, which is a diagonal area on the map. Breaking of odd chirality takes place in the outer zones of odd chirality. There are two types depending on the origin of fluctuation in the micro-MHD vortices: the red-B is induced by the vertical MHD flows on the micro-electrodes, and the pink-B is induced by the low magnetic fields. Achirality is in the outer zones of broken odd chirality.



**Figure 10.** Mapping of chiral symmetry on the axes of magnetic field vs. electrode diameter  $d$  (logarithmic scales). O: odd chirality; B: breaking of odd chirality; A: achirality. Adopted from [48].

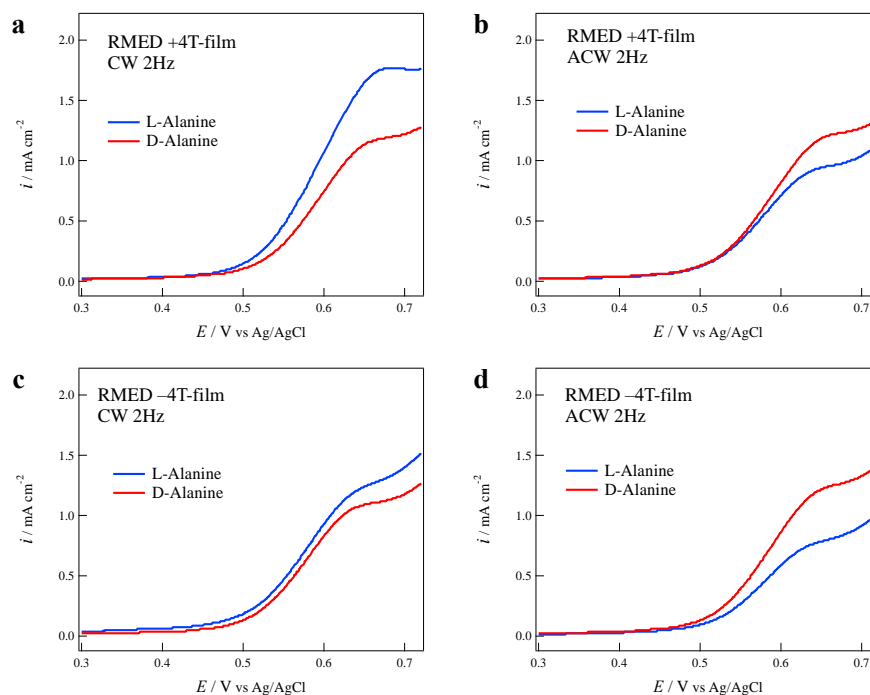
### 3.4. Effects of Cell Rotation

The rotation of electrodeposition cells in magnetic fields brings about the precession of micro-MHD vortices through the Coriolis force, as shown in Figure 11, and such precessions are asymmetric between the clockwise and anticlockwise vortices. Thereby, the rotational MED (RMED) can produce chiral surfaces, and their chiral signs depend on both the magnetic field polarity and the rotational direction [50].



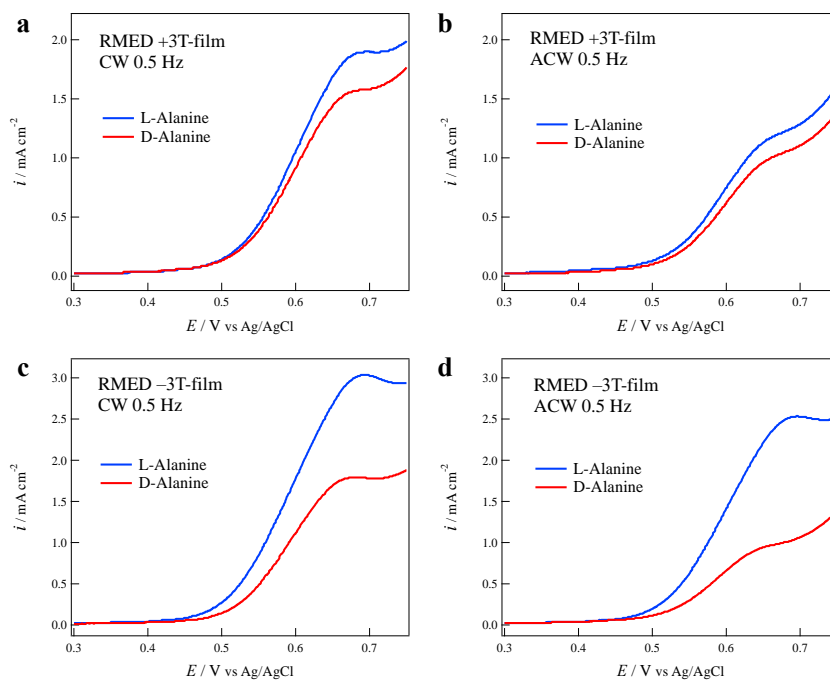
**Figure 11.** Effects of cell rotation on the micro-MHD vortices.

Figure 12 shows the voltammograms of alanine enantiomers on the {4T, 2 Hz} film electrodes. The two CW films show L-activity (Figure 12a,c), and the two ACW films show D-activity (Figure 12b,d). This means that the chiral signs of {4T, 2 Hz} films are controlled by the rotational direction, namely, they exhibit odd chirality for the rotational direction. On the other hand, the chiral signs of {3T, 6 Hz}, {2T, 4 Hz}, and {2T, 6 Hz} films also showed [2L + 2D] active patterns, but they exhibited odd chirality for the magnetic field polarity. This fact indicates that the vertical MHD flows penetrate into the tube around the electrode and affect the micro-MHD vortices. In several films, for example {2T, 0.5 Hz}, {5T, 6 Hz}, etc., both effects of rotation and vertical MHD flows were superimposed, then [3L + D] or [L + 3D] active patterns were observed. Thus, these films exhibit odd chirality for both rotational direction and magnetic field polarity.



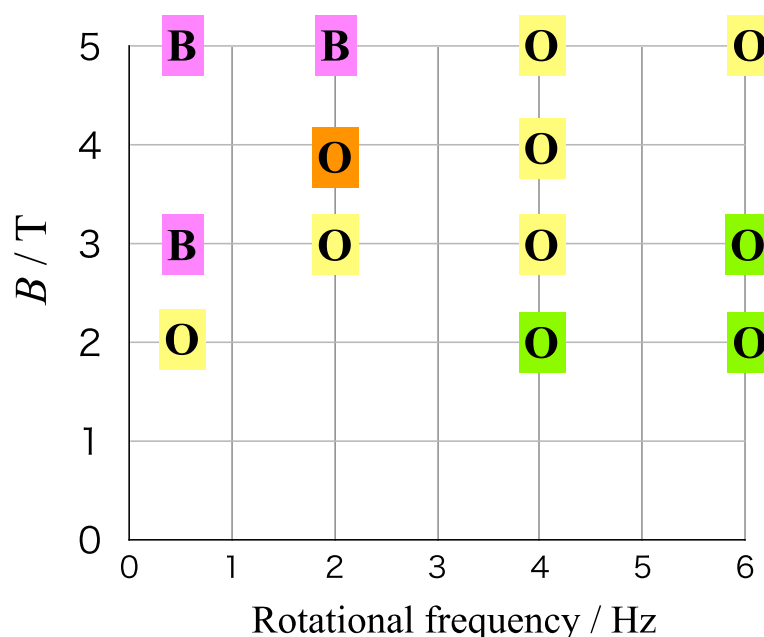
**Figure 12.** Voltammograms of alanine enantiomers in a 0.1 M NaOH aqueous solution on the RMED film electrodes: (a); +4T films, CW 2 Hz, (b); +4T films, ACW 2 Hz, (c); −4T films, CW 2 Hz, and (d); −4T films, ACW 2 Hz. Adopted from [50].

Figure 13 shows the voltammograms of alanine enantiomers on the {3T, 0.5 Hz} film electrodes. It is surprising that all four films show L-activity. This means that the {3T, 0.5 Hz} films exhibit breaking of odd chirality for both rotational direction and magnetic field polarity. Similar broken odd chirality was observed in the {5T, 0.5 Hz} and {5T, 2 Hz} films.



**Figure 13.** Voltammograms of alanine enantiomers in a 0.1 M NaOH aqueous solution on the RMED film electrodes: (a); +3T films, CW 0.5 Hz, (b); +3T films, ACW 0.5 Hz, (c); −3T films, CW 0.5 Hz, and (d); −3T films, ACW 0.5 Hz. Adopted from [50].

The chiral symmetry of RMED films is mapped on the axes of the magnetic field and the rotational frequency, as shown in Figure 14. The odd chirality is classified into three types depending on the rotational direction (orange-O), the magnetic field polarity (green-O), and both (yellow-O). The green-O appears in a zone of high rotational frequencies and low magnetic fields. As the frequency decreases and the magnetic field increase, the rotational effects become dominant; then, the orange-O appears in the {4T, 2 Hz} films. It is noteworthy that the breaking of odd chirality appears around the orange-O in the zone of lower frequencies and higher magnetic fields. If the rotational effects on the micro-MHD vortices are too strong, the precessions of micro-MHD vortices could be incoherent with each other, leading to the fluctuation of the self-organized state of micro-MHD vortices. As observed in the MED films, such fluctuation induces the breaking of odd chirality.



**Figure 14.** Mapping of chiral symmetry on the axes of magnetic field vs. the rotational frequency. O: odd chirality and B: breaking of odd chirality. Adopted from [50].

### 3.5. Breaking of Odd Chirality in Magnetochemical Etching

Chiral surfaces were produced by magnetochemical etching (MEE) of copper films [61,62]. Odd chirality was observed at 5 T on 3 mm electrodes [61], whereas breaking of odd chirality appeared in the MEE conditions with low magnetic fields [46], chloride additives [62], and micro-electrodes [48]. The self-organized states of micro-MHD vortices could also be formed in the MEE processes, and the fluctuation of micro-MHD vortices induces the breaking of odd chirality. The behavior of chiral symmetry in the MEE films is almost the same as that in the MED films. This fact implies a universal relation between the chiral symmetry and the fluctuation of micro-MHD vortices.

## 4. Conclusions

This paper has surveyed the chiral symmetry of MED films prepared with chloride additives (Figure 7), micro-electrode (Figure 10), and cell rotation (Figure 14). The mappings of chiral symmetry prove that odd chirality exists in the confined areas, where the rigid self-organized states of micro-MHD vortices are formed. This fact means that odd chirality can be easily broken by disturbances, which could induce the fluctuation of micro-MHD vortices.

In the mappings of chiral symmetry, breaking of odd chirality surrounds odd chirality, and achirality is more outside. The relatively gentle fluctuation of micro-MHD vortices causes the breaking of odd chirality, and the random fluctuation causes the disappearance

of surface chirality. In the states of broken odd chirality, the fact that the MED films exhibit the surface chirality indicates the ordered states in the fluctuation of micro-MHD vortices. Such ordered fluctuation could be crucial for the breaking of odd chirality.

In future studies, it is of great interest to explore how the ordered fluctuation is and how it breaks chiral symmetry. These issues would lead to hints for chiral symmetry breaking in nature and the origin of homochirality in biomolecules.

**Author Contributions:** I.M. and R.A. conceived and designed the concept and experiments; I.M., R.M., and K.T. conducted the experiments; K.T. contributed to superconducting magnet tools; I.M. wrote the paper. All authors have read and agreed to the published version of the manuscript.

**Funding:** This research was funded by JSPS KAKENHI Grant-in-Aid for Scientific Research (C) No. 19K05230.

**Institutional Review Board Statement:** Not applicable.

**Informed Consent Statement:** Not applicable.

**Acknowledgments:** The authors thank the staff members of the High Field Laboratory for Superconducting Materials of IMR Tohoku University for the use of the cryocooled superconducting magnet.

**Conflicts of Interest:** The authors declare no conflict of interest.

## References

1. Fahidy, T.Z. Magneto-electrolysis. *J. Appl. Electrochem.* **1983**, *13*, 553–563. [[CrossRef](#)]
2. Fahidy, T.Z. Hydrodynamic Models in Magneto-electrolysis. *Electrochim. Acta* **1973**, *18*, 607–614. [[CrossRef](#)]
3. Mohanta, S.; Fahidy, T.Z. Mass Transfer in a Magneto-electrolytic Flow Cell. *Electrochim. Acta* **1974**, *189*, 835–840. [[CrossRef](#)]
4. Aogaki, R.; Fueki, K.; Mukaibo, T. Application of Magneto-hydrodynamic Effect to the Analysis of Electrochemical Reaction. *Electrochemistry* **1975**, *43*, 504–514.
5. Monzon, L.M.A.; Coey, L.M.D. Magnetic Fields in Electrochemistry: The Lorentz Force. *Electrochem. Commun.* **2014**, *42*, 38–41. [[CrossRef](#)]
6. Tacken, R.A.; Janssen, L.J.J. Applications of Magneto-electrolysis. *J. Appl. Electrochem.* **1995**, *25*, 1–5. [[CrossRef](#)]
7. Iwakura, C.; Edamoto, T.; Tamura, H. Effect of a Relatively Weak Magnetic Field on Electrochemical Reactions. *J. Electrochem. Soc. Jpn.* **1984**, *52*, 596–601. [[CrossRef](#)]
8. Mohanta, S.; Fahidy, T.Z. The Effect of a Uniform Magnetic Field on Mass Transfer in Electrolysis. *Can. J. Chem. Eng.* **1972**, *50*, 248–253. [[CrossRef](#)]
9. Dash, J.; King, W.W. Electrothinning and Electrodeposition of Metals in Magnetic Fields. *J. Electrochem. Soc.* **1972**, *119*, 51–56. [[CrossRef](#)]
10. O'Brien, R.N.; Santhanam, K.S.V. Magnetic Field Effects on the Growth of the Diffusion Layer at Vertical Electrodes during Electrodeposition. *J. Electrochem. Soc.* **1982**, *129*, 1266–1268. [[CrossRef](#)]
11. Olivier, A.; Chopart, J.P.; Douglade, J.; Gabrielli, C. Investigation of Magnetic Effects on Mass Transport at the Electrode/Electrolyte Interface by Impedance Techniques. *J. Electroanal. Chem. Interfacial Electrochem.* **1987**, *217*, 443–452. [[CrossRef](#)]
12. Hinds, G.; Coey, J.M.D.; Lyons, M.E.G. Magneto-electrolysis of Copper. *J. Appl. Phys.* **1998**, *83*, 6447–6449. [[CrossRef](#)]
13. Mogi, I.; Okubo, S.; Nakagawa, Y. Dense Radial Growth of Silver Metal Leaves in a High Magnetic Field. *J. Phys. Soc. Jpn.* **1991**, *60*, 3200–3202. [[CrossRef](#)]
14. Mogi, I.; Kamiko, M.; Okubo, S.; Kido, G. Pattern Formation of Electrodeposit of Zinc in Magnetic Fields. *Phys. B Condens. Matter* **1994**, *201*, 606–610. [[CrossRef](#)]
15. Ni Mhiochain, T.R.; Coey, J.M.D. Chirality of Electrodeposits Grown in a Magnetic Field. *Phys. Rev. E* **2004**, *69*, 061404. [[CrossRef](#)] [[PubMed](#)]
16. Coey, J.M.D.; Hinds, G.; Lyons, M.E.G. Magnetic-Field Effects on Fractal Electrodeposits. *Europhys. Lett.* **1999**, *47*, 267–272. [[CrossRef](#)]
17. Heresanu, V.; Ballou, R.; Molho, P. Electrochemical Growth of Zn and Fe Arborescences under Normal Magnetic Field. *Magneto-hydrodynamics* **2003**, *39*, 461–468.
18. Heresanu, V.; Ballou, R.; Molho, P. Electrochemical Deposition of Iron in a Thin Cell under an In-Plane Magnetic Field. *Magneto-hydrodynamics* **2006**, *42*, 403–408.
19. Hirota, N.; Hara, S.; Uetake, H.; Nakamura, H.; Kitazawa, K. In Situ Microscopic Observations of an Electroless Silver Deposition Process under High Magnetic Fields. *J. Cryst. Growth* **2006**, *286*, 465–469. [[CrossRef](#)]
20. Bodea, S.; Vignon, L.; Ballou, R.; Molho, P. Electrochemical Growth of Iron Arborescences under In-Plane Magnetic Field: Morphology Symmetry Breaking. *Phys. Rev. Lett.* **1999**, *83*, 2612–2615. [[CrossRef](#)]
21. Katsuki, A.; Watanabe, S.; Tokunaga, R.; Tanimoto, Y. The Effects of High Magnetic Field on the Deposition of Silver. *Chem. Lett.* **1996**, *25*, 219–220. [[CrossRef](#)]

22. Katsuki, A.; Tanimoto, Y. Precession of Silver Dendrites in a Magnetic Field Due to MHD Induced Convection. *Chem. Lett.* **2005**, *34*, 726–727. [[CrossRef](#)]
23. Fahidy, T.Z. Characteristics of Surfaces Produced via Magneto-electrolytic Deposition. *Prog. Surf. Sci.* **2001**, *68*, 155–188. [[CrossRef](#)]
24. Duan, W.; Kitamura, S.; Uechi, I.; Katsuki, A.; Tanimoto, Y. Three-dimensional morphological chirality induction using high magnetic fields in membrane tubes prepared by a silicate garden reaction. *J. Phys. Chem. B* **2005**, *109*, 13445–13450. [[CrossRef](#)] [[PubMed](#)]
25. Yokoi, H.; Kuroda, N.; Kakudate, Y. Magnetic field induced helical structure in freestanding metal silicate tubes. *J. Appl. Phys.* **2005**, *97*, 10R513. [[CrossRef](#)]
26. Mogi, I.; Kamiko, M. Pattern Formation in Magneto-electropolymerization of pyrrole. *J. Electrochem. Soc. Jpn.* **1996**, *64*, 842–844. [[CrossRef](#)]
27. Tanimoto, Y.; Shinyama, A.; Omote, K. Three-Dimensional Morphological Chirality Induction in Polythiophene Polymer Deposit Using a Magnetic Field. *Bull. Chem. Soc. Jpn.* **2009**, *82*, 695–697. [[CrossRef](#)]
28. Rikken, G.L.J.A.; Folling, J.; Wyder, P. Electrical Magnetochiral Anisotropy. *Phys. Rev. Lett.* **2001**, *87*, 236602. [[CrossRef](#)]
29. Mogi, I.; Watanabe, K. Chirality of Magneto-electropolymerized Polyaniline Electrodes. *Jpn. J. Appl. Phys.* **2005**, *44*, L199–L201. [[CrossRef](#)]
30. Mogi, I.; Watanabe, K. Electrocatalytic Chirality on Magneto-Electropolymerized Polyaniline electrodes. *J. Solid State Electrochem.* **2007**, *11*, 751–756. [[CrossRef](#)]
31. Kumar, A.; Mondal, P.C.; Fontanesi, C. Chiral Magneto-Electrochemistry. *Magnetochemistry* **2018**, *4*, 36. [[CrossRef](#)]
32. Gazzotti, M.; Arnaboldi, S.; Grecchi, S.; Giovanardi, R.; Cannio, M.; Pasquali, L.; Giacomino, A.; Abollino, O.; Fontanesi, C. Spin-Dependent Electrochemistry: Enantio-Selectivity Driven by Chiral-Induced Spin Selectivity Effect. *Electrochim. Acta* **2018**, *286*, 271–278. [[CrossRef](#)]
33. Mogi, I.; Watanabe, K. Chiral electrode behavior of magneto-electrodeposited silver films. *ISIJ Int.* **2007**, *47*, 585–587. [[CrossRef](#)]
34. Mogi, I.; Watanabe, K. Magneto-electrochemical Chirality in Ag Electrodeposition. *J. Chem. Chem. Eng.* **2010**, *4*, 16–22.
35. Mogi, I.; Watanabe, K. Chiral recognition of amino acids by magneto-electrodeposited Cu film electrodes. *Int. J. Electrochem.* **2011**, *2011*, 239637. [[CrossRef](#)]
36. Mogi, I.; Watanabe, K. Chirality of magneto-electrodeposited Cu films. *Magnetochemistry* **2012**, *48*, 251–259.
37. Mogi, I.; Watanabe, K. Enantioselective recognition of tartaric acid on magneto-electrodeposited copper film electrodes. *Chem. Lett.* **2012**, *41*, 1439–1441. [[CrossRef](#)]
38. Aogaki, R. Micro-MHD effect on electrodeposition in the vertical magnetic field. *Magnetochemistry* **2003**, *4*, 453–460.
39. Aogaki, R.; Morimoto, R. Nonequilibrium Fluctuations in Micro-MHD Effects on Electrodeposition. In *Heat and Mass Transfer: Modeling and Simulation*; Hossain, M., Ed.; InTech: London, UK, 2011; pp. 189–216.
40. Mogi, I.; Iwasaka, K.; Aogaki, R.; Takahashi, K. Communication—Visualization of Magneto-hydrodynamic Micro-Vortices with Guanine Micro-Crystals. *J. Electrochem. Soc.* **2017**, *164*, H584–H586. [[CrossRef](#)]
41. Daltin, A.L.; Chopart, J.P. Magnetic Field Effect on Electrodeposition of Cu<sub>2</sub>O Crystals. *Magnetochemistry* **2009**, *45*, 267–273. [[CrossRef](#)]
42. Sommeria, J.; Meyers, S.D.; Swinney, H.L. Laboratory Simulation of Jupiter’s Great Red Spot. *Nature* **1988**, *331*, 689–693. [[CrossRef](#)]
43. Marcus, S.M. Numerical Simulation of Jupiter’s Great Red Spot. *Nature* **1988**, *331*, 693–696. [[CrossRef](#)]
44. Yanson, Y.I.; Rost, M.J. Structural Accelerating Effect of Chloride on Copper Electrodeposition. *Angew. Chem. Int. Ed.* **2013**, *52*, 2454–2458. [[CrossRef](#)] [[PubMed](#)]
45. Mogi, I.; Aogaki, R.; Watanabe, K. Tailoring of Surface Chirality by Micro-Vortices and Specific Adsorption in Magneto-electrodeposition. *Bull. Chem. Soc. Jpn.* **2015**, *88*, 1479–1485. [[CrossRef](#)]
46. Mogi, I.; Aogaki, R.; Takahashi, K. Fluctuation Effects of Magneto-hydrodynamic Micro-Vortices on Odd Chirality in Magneto-electrolysis. *Magnetochemistry* **2020**, *6*, 43. [[CrossRef](#)]
47. Mogi, I.; Aogaki, R.; Takahashi, K. Chiral Surface Formation in Magneto-electrolysis on Micro-Electrodes. *Magnetochemistry* **2017**, *53*, 321–328. [[CrossRef](#)]
48. Mogi, I.; Aogaki, R.; Takahashi, K. Breaking of Odd Chirality in Magneto-electrodeposition of Copper Films on Micro-Electrodes. *Magnetochemistry* **2021**, *7*, 142. [[CrossRef](#)]
49. Mogi, I.; Morimoto, R.; Aogaki, R. Surface Chirality Effects Induced by Magnetic Fields. *Curr. Opin. Electrochem.* **2018**, *7*, 1–6. [[CrossRef](#)]
50. Mogi, I.; Morimoto, R.; Aogaki, R.; Takahashi, K. Surface Chirality in Rotational Magneto-electrodeposition of Copper Films. *Magnetochemistry* **2019**, *5*, 53. [[CrossRef](#)]
51. Wachterhauser, G. Before Enzyme and Templates: Theory of Surface Metabolism. *Microbiol. Rev.* **1988**, *52*, 452–484. [[CrossRef](#)]
52. Switzer, J.A.; Kothari, H.M.; Poizot, P.; Nakanishi, S.; Bohannan, E.W. Enantiospecific Electrodeposition of a Chiral Catalyst. *Nature* **2003**, *425*, 490–493. [[CrossRef](#)] [[PubMed](#)]
53. Attard, G.A.; Harris, C.; Herrero, E.; Feliu, J. The Influence of Anions and Kink Structure on the Enantioselective Electro-Oxidation of Glucose. *Faraday Discuss.* **2002**, *121*, 253–266. [[CrossRef](#)] [[PubMed](#)]
54. Attard, G.A.; Ahmadi, A.; Jenkins, D.J.; Hazzazi, O.A.; Wells, P.B.; Griffin, K.G.; Johnston, P.; Gillies, J.E. The Characterisation of Supported Platinum Nanoparticles on Carbon Used for Enantioselective Hydrogenation: A Combined Electrochemical-STM Approach. *ChemPhysChem* **2003**, *4*, 123–130. [[CrossRef](#)] [[PubMed](#)]

55. Gellman, A.J.; Horvath, J.D.; Buelow, M.T. Chiral Single Crystal Surface Chemistry. *J. Mol. Catal. Chem.* **2001**, *167*, 3–11. [[CrossRef](#)]
56. Luo, P.; Zhang, F.; Baldwin, R.P. Constant Potential Amperometric Detection of Underivatized Amino Acids and Peptides at A Copper Electrode. *Anal. Chem.* **1991**, *63*, 1702–1707. [[CrossRef](#)]
57. Shao, W.; Pattanaik, G.; Zangari, G. Influence of Chloride Anions on Mechanism of Copper Electrodeposition from Acidic Sulfate Electrolytes. *J. Electrochem. Soc.* **2007**, *154*, D201–D207. [[CrossRef](#)]
58. Kao, Y.L.; Li, K.C.; Tu, G.C.; Huang, C.A. Microstructural Study of the Effect of Chloride Ion on Electroplating of Copper in Cupric Sulfate-Sulfuric Acid Bath. *J. Electrochem. Soc.* **2005**, *152*, C605–C611. [[CrossRef](#)]
59. Dow, W.P.; Huang, H.S. Roles of Chloride Ion in Microvia Filling by Copper Electrodeposition. *J. Electrochem. Soc.* **2005**, *152*, C67–C76. [[CrossRef](#)]
60. Nagy, Z.; Blaudeau, J.P.; Hung, N.C.; Curtiss, L.A.; Zurawski, D.J. Chloride Ion Catalysis of the Copper Deposition Reaction. *J. Electrochem. Soc.* **1995**, *142*, L87–L89. [[CrossRef](#)]
61. Mogi, I.; Aogaki, R.; Watanabe, K. Chiral Surface Formation of Copper Films by Magnetochemical Etching. *Magnetochemistry* **2015**, *51*, 361–368. [[CrossRef](#)]
62. Mogi, I.; Aogaki, R.; Takahashi, K. Chiral Symmetry Breaking in Magnetochemical Etching with Chloride Additives. *Molecules* **2018**, *23*, 19. [[CrossRef](#)] [[PubMed](#)]